Mean flow of turbulent boundary layers over porous substrates

L. B. Esteban,* E. Rodríguez-López, M. A. Ferreira, and B. Ganapathisubramani†
Department of Aeronautics & Astronautics,
University of Southampton, Southampton, UK
(Dated: September 21, 2022)

Mean flow measurements of turbulent boundary layers over porous walls (permeable and rough) with varying pore size (s), permeability (K) and thickness (h) are presented across a wide range of friction Reynolds numbers ($Re_\tau \approx 2000-18000$) and permeability based Reynolds numbers ($Re_K \approx 1.5-60$). The mean wall shear stress was determined using a floating element drag balance and the boundary layer profiles were acquired using hot-wire anemometry. Substrate permeability is shown to increase the magnitude of the mean velocity deficit. The use of a modified indicator function, assuming "universal" values for von-Karman constant ($\kappa = 0.39$) supports previous results where a strongly modified logarithmic region was observed. The indicator function was also used to estimate the zero-plane displacement (y_d), the roughness function (ΔU^+) and equivalent sandgrain roughness (k_s). At high Reynolds numbers, the roughness function data collapses on to the Nikuradse's fully-rough asymptote. However, at low roughness Reynolds numbers ($k_s^+ < 100$), we observe the flow to be transitionally rough, evolving with Nikuradse-type behaviour. The equivalent sandgrain roughness k_s for each substrate appears to include roughness and permeability contributions. These two contributions can be separated using data obtained from the same substrates with different thickness. This may allow us to model the porous wall as a combination of rough and permeable wall.

INTRODUCTION

Porous boundaries are ubiquitous in most natural processes that surround us, such as atmospheric boundary layers over forest canopies, flow over bird feathers or water currents over river beds among others. Porosity also plays an important role in biology, controlling mass transfer through organic tissues such as blood vessels and the respiratory system in mammals. As these illustrative examples suggest, a better understanding of the interaction of porous media with turbulent flows would have a positive impact in a wide variety of fields, spanning from aeronautics to biology.

There is a lack of understanding on how porous substrates modify the well known turbulent boundary layer that develops over them. The shift of the logarithmic law near the wall and its dependence on the porous material properties is still unclear. Besides, it is still unknown to what extent turbulent boundary layers over porous media are similar to boundary layers over rough walls. If this analogy can be made, correlations for the increase in skin friction with substrate properties could be obtained as for rough walls, as in Ref. [1–3].

There are only a few models that can predict how a porous substrate of known geometry influences the mean flow field and turbulent statistics [4, 5]. Although the number of experimental and numerical datasets of turbulent flows over porous media are rapidly increasing, these are still very limited in terms of Reynolds number (Re), pore size (s) (or filament thickness of the porous medium (l)) and permeability (K). Note that some of these geometric parameters are related to each other (for example, for the foams used here, different combinations of pore size and filament thickness can lead to a foam with the same permeability). Also, previous experimental datasets are limited in the sense that friction velocity is not directly obtained from an independent measure but inferred from other turbulent quantities, and this represents a strong limitation when certain assumptions are to be scrutinized. On the other hand, numerical simulations have been restricted to low to moderate Reynolds numbers, where the scale separation between outer and inner length scales might not be sufficient.

In addition, almost all previous studies on turbulent flow over porous substrates have employed relatively thick media, such that flow penetration into the substrate depends only on pore size or permeability, as in Ref. [6]. However, many situations involve finite thickness porous substrates bounded by a impermeable boundary, as identified in Ref. [7], and the substrate thickness (h) relative to the boundary layer thickness (δ) and/or the mean pore size (s) becomes a relevant factor. In fact, in the extreme scenario of thickness comparable to pore size ($h \approx s$) the substrate might be considered as a rough wall.

Previous studies

Previous experimental work on the effect of porous substrates started with flows over permeable beds of packed spheres [8]. In the aforementioned work, they observed an increase in skin friction for their open-channel facility compared with the impermeable

wall case and this was attributed to the additional energy dissipation caused by the exchange of momentum across the fluid-porous interface. Similarly, in Ref. [9] it was measured an increase in skin friction in boundary layers over porous walls made of sintered metals, bonded screen sheets and perforated titanium sheets. In wind-tunnel experiments of boundary layer flows over a bed of grains [10], it was also reported a rise in skin friction with respect to impermeable rough walls. A few years later, the flow induced in the transition layer, next to the porous-fluid interface, was investigated and it was concluded that permeability enhances momentum flux and Reynolds stresses near the interface [11].

More recently, PIV measurements on open channel flows were performed and velocity statistics of an impermeable wall of one layer of spheres was compared with a permeable wall composed of five layers [12]. In Ref. [6] it was highlighted the effect of wall permeability on the near-wall flow structure, suggesting that this is regulated by a competing mechanism between attached and shear instability eddies. Following a similar approach, other works have examined the effect of permeability over regularly packed spheres in a refractive-index-matched flow environment [13–15], exploring the independent roles of wall permeability and surface topology.

Experimental work in Ref. [7] based on Laser-Doppler velocimetry (LDV) measurements also showed a substantial modification of the turbulent boundary layer over highly-porous foams compared with the canonical smooth-wall case. They investigated the smooth to porous transition and found that the internal boundary layer was fully developed after 10δ from the porous transition, where δ is the boundary layer thickness. They also observed a wall-normal shift of the logarithmic region and a mean velocity deficit relative to the canonical smooth-wall profile. However, they were limited to a relatively small range of Reynolds number and pore size configurations ($7 < s^+ < 52$), where the superscript + stands for a quantity normalized by the friction velocity U_τ and the kinematic viscosity ν. Note that the magnitude of U_τ used in the former study was obtained from the smooth-wall region upstream of the porous substrate and does not include information about the effect of substrate permeability on the flow. Thus, it is expected to observe noticeable differences for surfaces with "same" normalized pore size (s^+) depending on the definition used.

One of the first direct numerical simulations (DNS) over a permeable surface was performed in Ref. [16]. In this work, they included an effective admittance coefficient to link the wall-pressure and wall-normal velocity in order to model the permeable interface. However, recent DNS studies have been focused in other strategies. Some have used the volume-averaged Navier–Stokes (VANS) equations, with the porous media modelled as cubical elements, as in Ref. [17, 18], whereas other DNS studies used interconnected cubes, as reported in Ref.[19, 20]. In Ref. [17, 21] it was suggested that a isotropic porous substrate could be fully defined by three length scales which are: 1) the square root of material permeability $\sqrt{K}$, 2) the substrate thickness h and 3) the characteristic size of the 'roughness' elements composing the substrate d_p.

Further, in Ref. [17] it was stated that the effect of permeability on the flow is isolated if three conditions are meet: i) the wall thickness is larger than the flow penetration into the substrate, ii) the roughness Reynolds number $Re_d = d_p U_\tau/\nu$ is small ($Re_d < 5$ - hydrodynamically smooth condition) and iii) the permeability

Reynolds number $Re_K = \sqrt{K}U_\tau/\nu$ is high ($Re_K > 1$). They performed DNS of channel flows over permeable walls meeting the aforementioned conditions and showed strong deviations in the structure and dynamics of wall turbulence. More precisely, they showed that as permeability increases, the high- and low-speed streaks associated with quasi-stream-wise vortices of smooth walls become less severe. They also fitted the logarithmic law of the wall to the mean velocity profiles and found a von-Karman coefficient (κ) considerably smaller than for smooth or rough walls. However, the authors suggested that this anomaly in the value of κ could be attributed to the low Reynolds numbers of the simulations. Similar trends were also observed in the simulations performed in Ref. [18] among others.

In Ref. [22] they also used a VANS formulation to study turbulent channel flows ($Re_\tau = 180$) over isotropic porous substrates but with the additional feature of being able to decouple porosity from permeability. Thus, they showed that low permeabilities can also lead to significant modification of the turbulent flow. On the contrary, the porosity of the substrate tested ($\epsilon = 0.3 - 0.9$) was found to alter the flow substantially less. Note that in the current study, $Re_\tau = \delta U_\tau/\nu$ is the friction Reynolds number based on boundary layer thickness.

A recent large-eddy simulation (LES) study in open-channel flow over sphere beds at Re_K up to 109 and $Re_d = dU_\tau/\nu$ up to 2900, where d stands for the sphere diameter, observed the existence of a transition from ejections-dominating to sweeps-dominating zone with vertical distance from the permeable beds and established an empirical correlation between the zero-plane displacement and the penetration depth [23].

Contrary to experimental studies, where most of the effort has been devoted to isotropic substrates, numerical studies have also explored a wide range of anisotropic configurations. In Ref. [24] they carried out Lattice Boltzmann simulations over anisotropic porous media in a modelled substrate in which the material permeabilities could be altered along the stream-wise, span-wise and wall-normal direction independently. Doing so, they showed that the stream-wise permeability can be tuned to hamper the high- and low-speed streaks of the near-wall cycle. Similarly, a DNS work on channel flows showed up to 25% turbulent drag reduction using anisotropic permeable substrates [25]. They observed that in the linear regime of small permeabilities the drag reduction is proportional to the difference between the virtual origin perceived by the mean flow and the one perceived by turbulence. Note that this was only achieved in configurations were the permeability was preferential in the stream-wise direction. In these situations, turbulence remains what the authors called "smooth-wall-like" but displaced towards the porous interface reducing the overall drag.

Substrates with irregular packing and multi-layer arrangements with different particle sizes have been also explored to investigate the effect of these configurations on the transport characteristics across the interface in Ref. [26–28]. Similarly, the permeability effects on turbulent channel flows over substrates comprising rib-type porous roughness have been also recently explored in Ref. [29].

As observed in turbulent flows over rough walls, previous studies over porous substrates have also found a logarithmic region in the mean velocity profile. The loga-

rithmic region is often parametrised as,

$$U^+ = \frac{1}{\kappa}\ln(y + y_d)^+ + B - \Delta U^+ \tag{1}$$

where κ and B are the von-Karman and additive constants respectively, y is the wall-normal distance from the porous upper surface, y_d is the shift of the logarithmic layer or zero-plane displacement and ΔU^+ the roughness function as in Ref. [30].

Fits of the experimental and numerical data of the mean velocity profiles to equation 1 have been carried out in previous studies to examine the validity of the logarithmic law of the wall. Results from the DNS study in Ref. [17] of turbulent channel flow over porous substrates suggested that the von-Karman constant decreases from $\kappa \approx 0.4$ (smooth-wall case) down to $\kappa \approx 0.23$ for the substrate with higher permeability. Similarly, in the experimental work in Ref. [31] they found the value of κ to decrease with increasing Reynolds number based on substrate permeability ($Re_K = U_\tau\sqrt{K}/\nu$). However, skin friction velocity (U_τ) was not directly measured but obtained by extrapolating the measured Reynolds shear stress distribution to the porous wall. In Ref. [6], they also found lower von-Karman coefficients than those reported for smooth and rough walls (from $\kappa = 0.33$ to 0.31) but significantly higher than in the aforementioned studies. The authors discussed that the behaviour of κ is therefore not fully captured by Re_K, and suggested that a poor separation between inner and outer scales might have affected the results in previous studies.

It was discussed in Ref. [6] that if one agrees with Ref. [32] on the zero-plane position (y_d) dependency with shear penetration, the ratio between inner and outer length scales could be captured, to some extent, by the relation y_d/δ. In fact, they showed a more consistent behaviour of κ versus y_d/δ than versus Re_K. Unfortunately, the shear penetration is not fully represented by the estimation of the zero-plane displacement and flow measurements within the porous media would be required for a better understanding. In Ref. [6], they also showed an attempt to scale the velocity profiles based on the substrate permeability (K). Nevertheless, they later proposed to use the roughness length (z_0) for this purpose, this being a function of both substrate permeability and a viscous length scale.

Contribution and outline

The present study extends the experiments carried out in Ref [6, 7] to provide further insight into the mean flow characteristics over porous substrates. The foams tested in this study are similar to those considered in the aforementioned studies and include three different pore sizes (s = 0.24, 0.89 and 3.84 mm) and two thicknesses (h = 3 and 15 mm). Hot wire anemometry (HW) measurements were performed to obtain streamwise velocity profiles over these foams at a range of Reynolds numbers together with drag balance measurements that provide a direct measure of skin friction velocity. The friction Reynolds number over the foams based on skin friction velocity (U_τ) and boundary layer thickness (δ) for the conditions tested was in the range $Re_\tau \approx 0.2 - 1.8 \times 10^4$ and the permeability Reynolds number (Re_K) was in the range

$Re_K \approx 1.6 - 63$. To our knowledge, this represents the broadest range of Reynolds numbers tested for turbulent boundary layer over porous walls up to date. Over this range, we expect both permeability of the surface and roughness of the top surface to play a crucial role in the determination of drag incurred by the surface. We aim to utilise the data to develop a framework where the contributions from the permeability can be decoupled from that of roughness. Overall, we aim to develop a new framework to understand the drag incurred by porous rough surfaces.

The paper is structured as follows: First, the paper describes the experiments, giving details of the facility, porous substrates and experimental techniques; then, the paper focuses on the experimental results, showing the independent measure of skin friction from the drag balance and shows mean velocity profiles from hot wire measurements. Subsequently, the paper discusses mean velocity profiles from a rough-wall framework, to later present estimates of equivalent sandgrain roughness assuming "universal" value of the von-Karman constant ($\kappa = 0.39$). Using this framework, we also attempt to separate the effects of roughness from that of permeability.

EXPERIMENTAL SETUP AND MEASUREMENT TECHNIQUES

Porous substrate

Turbulent boundary layer measurements were performed over three different kinds of porous substrates and two different thicknesses for each kind. All of these substrates are open-cell reticulated polyurethane foam with porosity (empty volume over total volume) of approximately $\epsilon \approx 0.96 - 0.98$. Pictures of 3mm thick substrates mounted on a flat plate are shown in figure 1. The porosities of these substrates were measured by measuring the weight of the porous surface with a given sample size (using a scale with a precision of 0.001g) and comparing that to a solid block of the same sample size. These weight measurements were repeated for different sample sizes and consistent porosity values were obtained. Other methods were also used to measure porosities but provided inconsistent results and therefore we report the value obtained only from the weight/mass measurements. A small sample of all substrates was also scanned (CT-scan) with a voxel resolution of 0.056 mm in all three dimensions. The data was imported into the open source FijiJ software and the commercial Avizo software to estimate pore size. The mean pore size of the substrates were found to be $s \approx 3.84$, 0.89, 0.25 mm ordered from the most porous to the least porous substrate.

The other parameter of relevance in these substrates is permeability, which is an indicator of resistance to fluid flow through a porous medium. The permeability of each substrate was obtained by means of a standard 'Darcy-type' experiment as in Ref. [6], where a sample of the substrate was placed within a closed duct of circular cross-section and an air flow rate was imposed. To improve the signal to noise ratio of the pressure readings the length of the substrate material was extended up to 0.6 m for the most permeable substrate. The parameters of interest for the foams tested are included in table I.

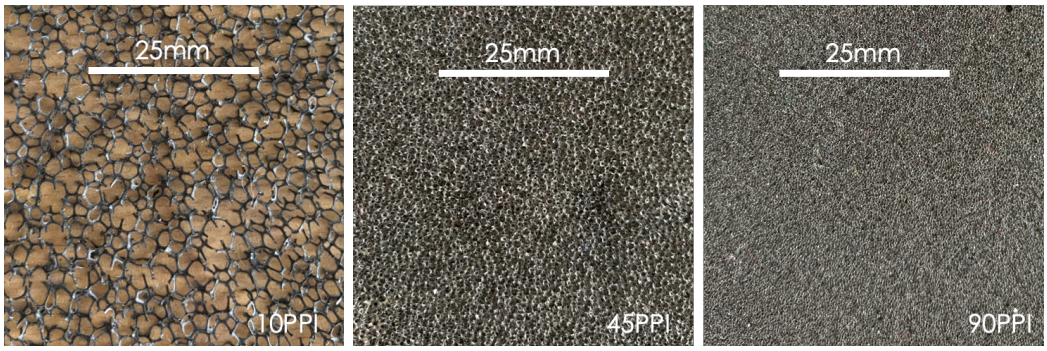

FIG. 1: Photographs of the 3mm thick porous substrates.

Foam (ppi)	s (mm)	K (10^{-9} m^2)	ϵ	h (mm)	Sym	h/s	$h/\sqrt{K}$
90	0.245	2.63	0.96	3	○	12.24	58.5
				15	●	61.22	292.5
45	0.89	36.2	0.97	3	☆	3.37	15.8
				15	★	16.85	78.8
10	3.84	245	0.98	3	◇	0.78	6.1
				15	◆	3.91	30.3

TABLE I: Physical properties of the foams. Porosity (ϵ) and average pore sizes (s) were obtained from the analysis of CT-scan data using Avizo and FijiJ software and permeability (K) was estimated from pressure drop experiments.

Facility

The experimental investigations were conducted in an open-circuit suction wind tunnel at the University of Southampton. The wind tunnel has a working section with a cross-plane of 0.9 m width and 0.6 m height, and of 4.5 m length. A turbulent boundary layer is developed over the bottom wall of the wind tunnel. The boundary layer is initially tripped at the beginning of the test section using P36 sandpaper (that is 100mm long). The rest of the test section length is covered with the the porous foam as shown in figure 2. The free stream velocity generated can reach up to 30 ms^{-1}, with less than 0.5% turbulence intensity, and is controlled through a National Instruments Data Acquisition system (NI-DAQ) and acquired using a FC510 manometer. To account for the air density variations, the temperature is also acquired, and its standard deviation for an average run ($1.5 - 2.5$ h for the boundary-layer profiles) is less than 0.25°C. The streamwise pressure gradient in the flow is assessed by traversing the pitot probe, which yielded an acceleration parameter $K_x = (\nu/U_\infty^2[dU_\infty/dx])$ of less than 1.5×10^{-8}

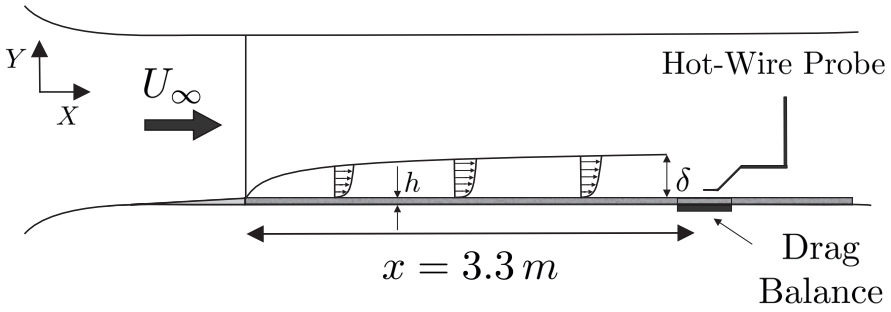

FIG. 2: Sketch of the experimental setup in the wind tunnel facility for drag balance and hot wire measurements over permeable substrates. The substrate thickness is represented with grey colour and the floating element drag balance (below the hot wire) is represented as a dark contour underneath the substrate. The thickness of the substrate is represented with h and the boundary layer thickness with δ.

(this value was the worst case across all measurements presented here). This suggests that there is indeed a mild favourable pressure gradient in the flow, however, previous works have indicated such values of acceleration parameter could be considered as nominally zero-pressure-gradient.

Hot Wire Anemometry

A single hot wire boundary-layer-type probe is used to measure the time series of the stream-wise velocity at different wall-normal locations and to determine the mean velocity profiles. The single wire probe had a 10 mm long prongs spanned by a 3 mm long and 5 μm diameter tungsten wire with a sensing length of about 1 mm. The resulting length-to-diameter ratio of the probe is 200 which follows the recommendation in Ref. [33]. A DANTEC Streamline Pro constant temperature anemometer (CTA) system was used and operated at fixed overheat ratio of 0.8. The turbulent boundary-layer profiles consisted of 46 wall-normal locations, each of which had an acquisition time of $3-5$ min, leading to a signal length (T) always greater than 20000 boundary layer turnover times ($TU_\infty/\delta > 20000$). The sampling rate was fixed at 20 kHz.

Drag Balance

Indirect methods to estimate surface shear stress are generally used to characterise boundary-layer flows. The problem with these methods are the large uncertainties, especially for surfaces where the validity of extant scaling and similarity laws are not established. Therefore, independent measurement techniques that can accurately measure skin friction are of paramount importance in these scenarios. In this work, we use the floating element balance presented in Ref. [34], for which the measurements

of skin-friction coefficient (C_f) for a smooth-wall boundary layer agree with values inferred from hot wire anemometry to within 2% ($Re_\theta > 4 \times 10^3$). The floating element balance is flush mounted with the wind tunnel floor and the gap surrounding the balance is taped over to prevent leaks. The porous foams are cut with 0.1 mm precision to accommodate on top of the balance surface. Note that this precision is within the size of a pore for all surfaces and therefore its effect on the flow should be minimal.

RESULTS

Mean surface shear stress

The following results from the floating element drag balance show the evolution of the skin friction ($C_f = 2U_\tau^2/U_\infty^2$) as a function of Reynolds number (Re_τ) for the six porous substrates investigated. Details of the surfaces investigated and the symbols that represent them can be found in table I.

The boundary layer thickness for the drag balance measurements are inferred from the boundary layer measurements carried with the hot wire at three unit Reynolds number $U_\infty/\nu \approx 6.6 \times 10^5$ m^{-1}, $U_\infty/\nu \approx 1.2 \times 10^6$ m^{-1} and $U_\infty/\nu \approx 1.7 \times 10^6$ m^{-1}. Figure 3a shows the hot wire measurements at the aforementioned low, mid and high unit Reynolds number (yellow, red and purple, respectively) and the interpolated Re_τ data points corresponding to the drag balance measurements (black), for which boundary layer thickness was not measured. These three colours will be used throughout this study to differentiate the hot wire data taken at low, mid and high unit Reynolds number. Note that this does not imply that the friction Reynolds number Re_τ is similar for each colour, since this magnitude depends on friction velocity (U_τ) and boundary layer thickness (δ), and both are highly altered by the characteristics of the substrate.

The evolution of the skin friction as a function of Re_τ for the smooth-wall case shown in figure 3b is found using the approach detailed in Ref. [35]. Figure 3b also shows the independent measurements of skin friction from the drag balance as a function of the inferred Reynolds number (Re_τ). The data points corresponding to porous substrates with 90 pores per inch (ppi) and 45 ppi, represented by circles and hexagonal stars respectively, show an increase in the friction coefficient (C_f) with increasing Re_τ and tending towards a plateau beyond$Re_\tau > 0.5 \times 10^4$. We believe this behaviour of the friction coefficient reflects the transition from transitionally rough to the fully rough regime, as first found for pipe flow with uniform sandgrain roughness [36, 37]. This transitionally rough regime does not seem to be present for the other flow-substrate configurations, where the friction coefficient is nearly constant throughout the entire range of Reynolds numbers tested.

In the following section we investigate the velocity profiles of the turbulent boundary layers obtained by hot wire measurements (details of the turbulent boundary layers measured using this technique can be found in table II). This analysis allows us to estimate the roughness function using the profiles and also see whether the shape of

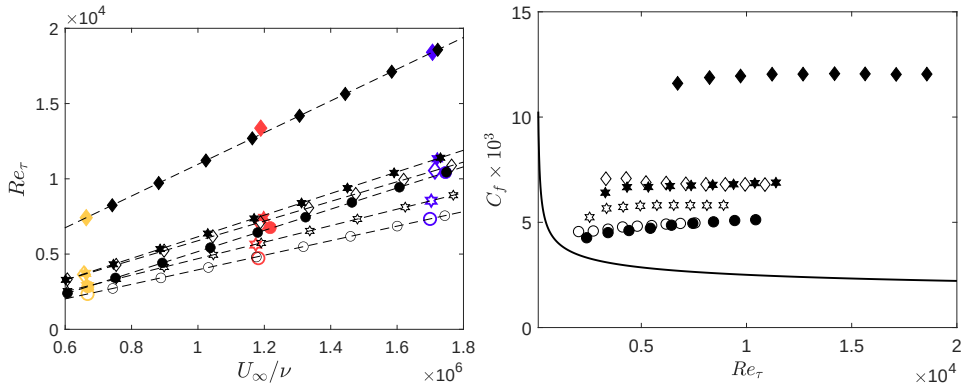

FIG. 3: (left - a) Re_τ data points corresponding to drag balance measurements (black) and the hot wire measurements (colour). (right - b) Skin friction coefficient (C_f) as a function of Re_τ. The solid line corresponds to the relation derived in Ref. [35] for the smooth-wall case. The symbols for the different permeable substrates as detailed in table II.

the mean velocity profiles in the overlap and outer region of the boundary layer are similar for smooth and porous walls.

Mean velocity profiles

Figure 4 contains the profiles of the mean stream-wise velocity scaled with inner variables, such that $U^+ = U/U_\tau$ and $y^+ = yU_\tau/\nu$, where the magnitude of U_τ is obtained from the direct measure of floating element drag balance. The origin for the wall-normal direction is the upper surface of the porous substrate and the base of the solid impermeable material is located at $y = -h$. Panels within figure 4 are arranged such that substrate porosity is kept constant in columns with increasing permeability from left to right, and substrate thickness is constant in rows with thin substrates ($h = 3\,mm$) on top panels and thick substrates ($h = 15\,mm$) at the bottom panels. All velocity profiles are plotted against the smooth-wall case for comparison, represented with black solid dots.

In the near-wall region, it can be observed that the velocity profiles have inflection and appear to asymptote to a constant value for some of the cases. The asymptotic value of the mean streamwise velocity near the wall can be considered as a proxy for the interfacial slip velocity at the porous interface and can be used to determine the onset/establishment of the effect of permeability, see Ref. [17, 31]. This inflection can be observed for the 15mm thickness case of 10ppi and is more obvious for all the other cases. This suggests that the wall has the characteristics of a permeable wall for these substrates compared to the 10ppi (3mm thickness) case where the profiles

s (mm)	h (mm)	K (10^{-9} m^2)	U_∞ (m/s)	Sym	δ (cm)	U_τ (m/s)	Re_τ	Re_K	s^+	ΔU^+	y_d (mm)	$k^+_{s_{HW}}$	$k_{s_{HW}}$ (mm)
0.245	3	2.63	10.4		7.41	0.494	2349	1.63	7.76	5.17	0.03	50.73	1.60
			18.5		8.25	0.896	4724	2.94	14.03	7.88	-0.15	91.74	
			26.7		8.88	1.301	7335	4.24	20.24	9.03	-0.31	132.30	
0.245	15	2.63	10.3		9.09	0.479	2831	1.60	7.63	5.19	-0.29	79.7	2.56
			17.8		10.67	0.926	6756	3.25	15.51	9.28	0.08	161.9	
			25.9		11.44	1.354	10415	4.67	22.30	10.48	-0.05	232.9	
0.89	3	36.2	10.3		8.44	0.528	2871	6.47	30.27	7.90	0.21	118.3	3.48
			18.3		9.14	0.959	5629	11.72	54.81	10.13	0.06	213.9	
			26.5		9.45	1.407	8545	17.20	80.47	11.25	0.18	314.4	
0.89	15	36.2	9.8		9.66	0.572	3716	7.32	34.23	10.47	0.86	301.6	7.97
			17.8		10.44	1.060	7436	13.55	63.39	12.60	1.05	557.9	
			25.8		11.05	1.534	11331	19.51	91.26	13.70	1.01	803.2	
3.84	3	245	9.8		9.21	0.591	3644	19.58	151.93	11.28	0.78	367.7	9.32
			17.8		9.94	1.056	7014	34.93	270.96	12.87	0.88	655.6	
			25.7		10.46	1.514	10549	49.92	387.26	14.05	1.01	936.9	
3.84	15	245	10.3		14.74	0.781	7417	24.90	193.22	15.91	4.78	2100	43.2
			18.4		14.71	1.410	13367	44.98	378.94	17.60	4.98	3791	
			26.5		14.14	2.025	18408	63.18	490.13	18.59	5.16	5429	

TABLE II: Details of the permeable wall hot wire data. The friction velocity (U_τ) is obtained from the direct measure of skin friction from the floating element drag balance.

resemble a rough-wall. Previous work has indicated that thickness of the substrate relative to the boundary layer thickness (δ/h) should be important in determining the importance of the permeability of the wall. For example, in Ref. [6] they reported values of δ/h approximately 1 while in Ref. [7] they reported values in the range of 5-6. In the current study, δ/h varies between 6-30 for different surfaces and therefore the flow is always under the influence of roughness and permeability to different extents. In addition to δ/h, the thickness of substrate relative to the pore size (h/s) is also important for permeability. Here, the range for h/s is from 0.8 (for 10 ppi) to 60 (for 90 ppi). The appearance of the asymptote near the wall for $h/s > 3$ (where $\delta/h \approx 30$) suggests that there should be a balanced between these length-scale ratios to determine the importance of permeability.

For sufficiently large values of h/s (> 10), the slip velocity tends to a constant at around $U^+ \approx$ 3-4. It should be noted that this slip velocity also appears to be a constant relative to the freestream velocity (approximately $0.2U_\infty$) for the same cases (not shown here for brevity). This is lower than previously reported observations in Ref. [7] who found a value of $0.3U_\infty$. They reported that the value of $0.3U_\infty$ is consistent with the value in Ref. [17] who found the slip velocity to be approximately $0.3U_b$ (U_b is the bulk velocity) in a channel flow (for a surface with similar porosity). Re-examination of the data from Ref. [17] with inner-scaling suggests that the inner-

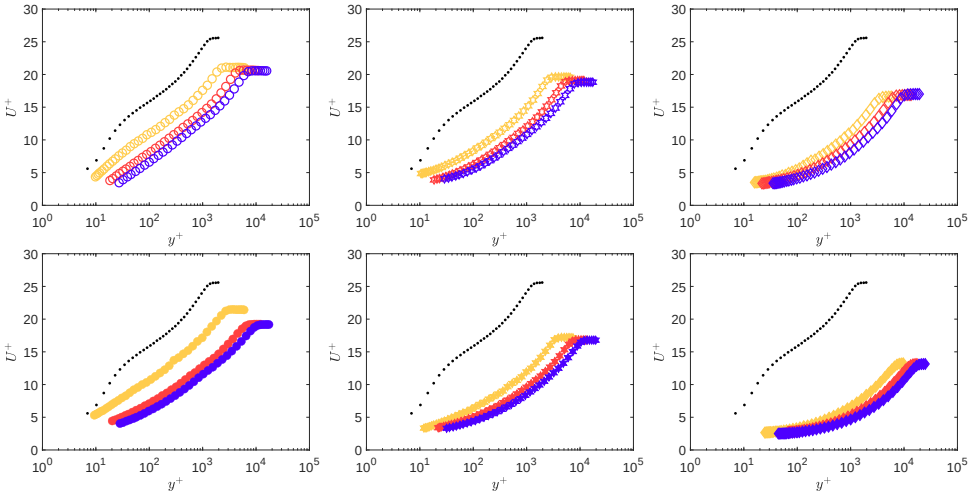

FIG. 4: Inner scaling of the mean stream-wise velocity profiles. Panels on the same row share substrate thickness ($h = 3$ mm top, $h = 15$ mm bottom), with the permeability of the substrate increasing from left to right. Each panel includes velocity profiles at three free-stream velocities and the smooth-wall case (represented with black solid dots) for comparison.

scaled slip velocity for the same data is about $U^+ \approx$ 4-5. This inner-scaled value is in fact similar to the values observed in the current study. This indicates that the slip velocity could scale with skin-friction rather than the freestream velocity. However, given the scatter and limited data, it is difficult to delineate the scaling, and it requires further work.

Farther away from the wall, We observe a downward shift of the profiles with increasing Reynolds number together with an apparent change in wake strength for increasing substrate permeability. A severe change in the overall shape of the velocity profiles is also noticeable, especially with increasing permeability. Specifically, an extended logarithmic region is not apparent. However, it is still possible to fit a log profile to the data, but, the wall-normal extent for a given log region is reduced with increasing permeability. Although we believe the flow dynamics close to the wall is not dominated by viscous effects, this normalisation allows us to show the progressive shift in the mean velocity (ΔU^+) with substrate characteristics. As discussed before, considering the worst case streamwise pressure gradient over the drag balance length, there is an uncertainty of 5% in the value of U_τ. This uncertainty is much smaller for all other cases. Further, another possible reason for the lack of profile collapse might come from the approach used to measure (or define) the friction velocity. It might be possible that a different candidate for the reference shear stress provides a friction velocity such that outer layer similarity is observed, but this is not the case when the direct measure of skin friction (pressure and viscous drag of the interface and within the substrate, plus solid wall contribution in case of flow penetration) is used for the

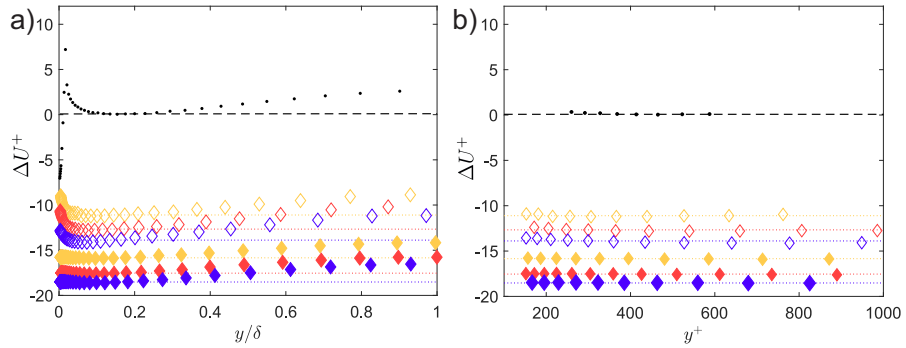

FIG. 5: a) Variation of the ΔU^+ function along the complete boundary layer profile. b) Variation of the ΔU^+ function for the overlap region in inner units. Each panel includes the smooth-wall case (represented with black solid dots) for comparison.

estimation of the skin friction velocity. This definition used of the friction velocity is consistent with that of a rough wall.

In previous studies, the mean flow profiles have been also used to fit a generic logarithmic expression with the value of κ free to float during the fitting optimization process. In contrast, in the following section, we aim to investigate the mean profiles applying the approaches generally used within the rough-wall framework.

Interpretation of mean velocity profiles based on a rough-wall framework

In this section we work with the mean velocity profiles as if these were obtained from rough wall measurements. We deduce the zero-plane displacement (y_d) following a different approach as the one presented in Ref. [6], and this consists on the subtraction of the log-layer profile (of the smooth-wall case with the addition of a virtual origin y_d) to the measured inner-normalized mean velocity profiles. To do so we define:

$$\Delta U^+ = U^+ - \frac{1}{\kappa}\ln(y^+ + {y_d}^+) - B \tag{2}$$

where U^+ corresponds to the experimental data over permeable walls and the von-Karman and additive constants are $\kappa = 0.39$, $B = 4.3$ as discussed in [38] in the context of turbulent boundary layers. Note that the magnitude of ΔU^+ will vary with wall normal distance; therefore we use the region of this quantity where the deviation from a straight line with zero slope is minimized (the overlap region) to extract its magnitude. The zero slope condition affects the goodness of the y_d fit, as will be discussed in due course, but this assumes the same κ as in smooth wall, and therefore here we impose the said zero slope condition.

Following this approach, the magnitude of the equivalent sandgrain roughness, that will be inferred from equation 3, can be related back to the smooth-wall case providing

comparability across substrates. The approach to estimate the zero-plane displacement is an alternative approach to the one followed in Ref. [17, 31], where they estimated y_d as the value that forces $(y + y_d)(\partial U/\partial y)$ to be constant over the overlap region. However, we favour the method used in the present study since the second approach relies on noisy velocity gradient data and the uncertainty in the fitted values was found to be considerably larger. Figure 5a shows the evolution of ΔU^+ across the boundary layer for all cases over the 10 ppi substrate, whereas figure 5b shows the data points corresponding to the overlap region in wall-units. The goodness of the fit in figure 5b provides evidence on the existence of a modified logarithmic region, and the same is observed for all porous substrates tested (not shown here).

In figure 6a, we show the estimated values of the dimensionless displacement height (y_d^+) as a function of Reynolds number based on substrate permeability (Re_K). The origin of the vertical axis corresponds to the flow-substrate interface, therefore negative values of the zero-plane displacement correspond to flow configurations where the zero-plane displacement is located over the substrate. The solid and dashed lines in figure 6 stand for the empirical relationships found for thick and thin substrates respectively. Note that these figures are plotted in linear axis to capture also the negative values of y_d. As previously discussed, the goodness of the fit for ΔU^+ would be slightly better when both κ and y_d are free to float during the optimization. This would lead to different combinations of the zero-plane displacement and κ; however, this scenario is not considered here. Also note that the negative values of the zero-plane displacement for the 90 ppi substrate suggest that this is located above the interface. This location differs from the results in the literature and might arise from the uncertainty in the estimation of U_τ or as an artefact from the fitting procedure, but do not conflict with the objective of the paper.

It is interesting to note that two of the conditions proposed in Ref. [17] to isolate the permeability effects are not met in this study. First, the condition $h/s >> 1$ to allow free flow penetration is not satisfied, and this ratio even becomes smaller than unity in one of the substrates tested. Second, the Reynolds number based on the pore diameter (s^+) (or filament diameter d^+) greatly exceeds the recommendation of $s^+ < 5$ and therefore roughness effects should not be neglected, see table II for more details.

To evaluate the roughness effect on the location of the zero-plane displacement we plot the evolution of the zero-plane displacement as a function of the Reynolds number based on pore diameter in figure 6b. It should be noted here that we use pore diameter as a representative scale for the roughness. However, choice of representative scale does not affect the results presented here. The zero-plane location still shows dependency on substrate thickness, however, there is considerable improvement on the goodness of the linear fit for both thicknesses.

We can now use the value ΔU^+ (shown in figure 5) to evaluate the change in the roughness function with increasing Reynolds number. This allows us to calculate the equivalent sandgrain roughness ([36]) as,

$$\Delta U^+ = \frac{1}{\kappa} \ln k_s^+ + B - B'_{FR} \tag{3}$$

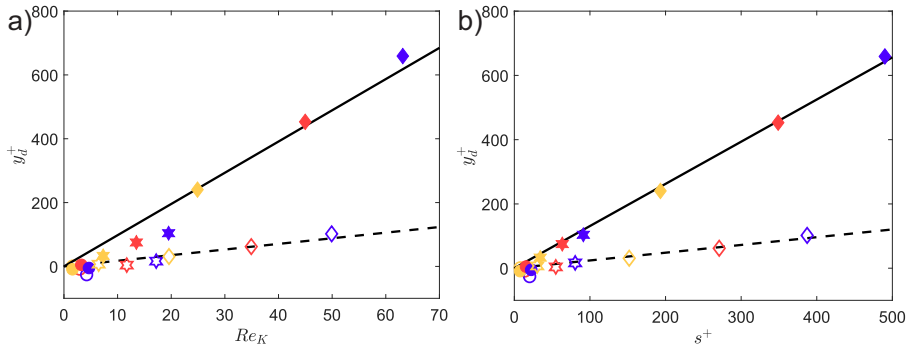

FIG. 6: a) Estimated dimensionless displacement height (y_d^+) as a function of the permeability Reynolds number (Re_K). The solid black line represents the empirical correlation for thick substrates ($y_d^+ = 9.78Re_K$) and the dashed black line the correlation for thin substrates ($y_d^+ = 1.76Re_K$). b) Estimated displacement height (y_d^+) as a function of the Reynolds number based on the pore diameter (s^+). The solid black line represents the empirical correlation for thick substrates ($y_d^+ = 1.31s^+$) and the dashed black line the correlation for thin substrates ($y_d^+ = 0.24s^+$).

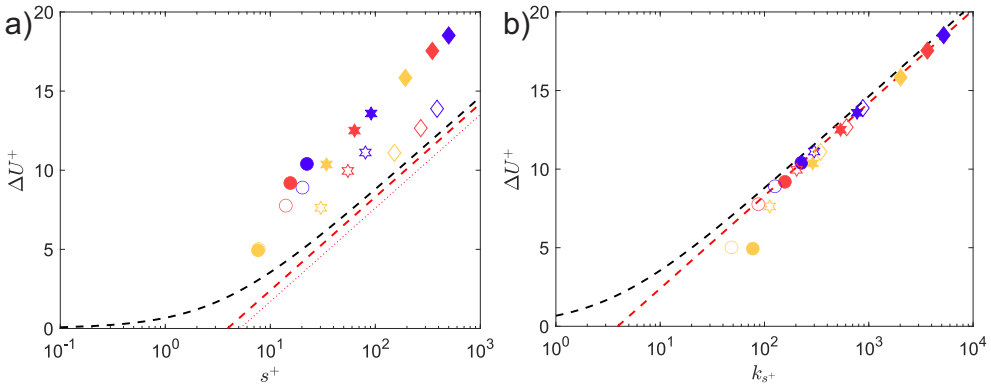

FIG. 7: Roughness function results where ΔU^+ is determined as in figure 5. The black dashed line corresponds to [37] relation, the red dotted line and dashed line represent the fully rough asymptote in [36] with the boundary layer constants found in [38] and $B'_{FR} = 8.5$ and 7.8 respectively.

Here, instead of using the von Karman constant and intercept found in Ref. [36], we use the analogous pair of constants for turbulent boundary layers as in Ref. [38]. Then, we follow the approach in Ref. [30] where $B - B'_{FR} = 3.5$ and therefore adapt the value of B'_{FR} to 7.8 to prevent excessive departure from the asymptote and to be consistent with the literature.

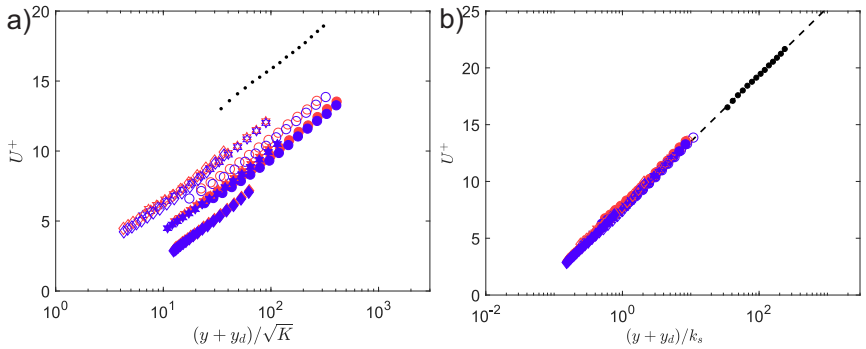

FIG. 8: a) Mean velocity profiles with the vertical coordinate scaled with the wall permeability. (b) Mean velocity profiles with the vertical coordinate scaled with the equivalent sandgrain roughness (k_s). Smooth wall data is plotted for reference (black dots) always scaled in viscous units.

This is performed for all the substrates and flow configurations tested and the results are plotted in figure 7a as a function of dimensionless pore size (s^+). We observe a nearly logarithmic increase in the roughness function with dimensionless pore size, regardless of the substrate examined. The equivalent sand-grain roughness can be obtained by shifting the data to coincide with the fully-rough asymptote as shown in figure 7b. When the roughness Reynolds number is small ($k_s^+ < 100$) the evolution of the roughness function resembles the one observed in transitionally rough scenarios, whereas for higher roughness Reynolds number the collapse of the data on the fully-rough asymptote is good. As commented for the drag balance data, we observe that these substrates behave as Nikuradse-type roughness, where the roughness function tends to zero for a finite value of k_s^+.

From the above figures, the equivalent sandgrain roughness (k_s) for each substrate based on the velocity profiles can be determined and these are included in table II. As previously discussed, the benefits of allowing κ to be optimized are not obvious when the results are to be put into context with the smooth-wall and rough-wall cases (with fixed κ). In order to enable this comparison we favour the present approach where κ is fixed at a "universal" value. Further, the good collapse of the data over the fully rough asymptote (see figure 7) suggests that porous surfaces can be modelled in a framework similar to rough surfaces using the equivalent sandgrain roughness.

The flow characteristics ($Re_K > 1$ and $s^+ > 5$) are such that permeability and roughness effects should both be present for these substrates. We can attempt to delineate between the two effects by examining the effects of permeability and roughness separately. Figure 8a shows the mean profile scaled with permeability ($\sqrt{K}$). The data shows good collapse across different speeds for individual substrates. However, we do not observe a direct dependency between the vertical shift of the logarithmic region and the permeability Reynolds number (Re_K), as was discussed in Ref. [6]. However,

there is very little difference in Re_K values between the thick and thin substrates (see table II). This suggests that permeability between the two sets of substrates might have saturated and any further differences are due to roughness.

On the other hand, 8b shows the the velocity profiles scaled with equivalent sand-grain roughness obtained using hot-wire data (k_s). The data here by definition has to show good collapse (and it does), but, it is important to consider that contrary to purely rough walls this length scale comes from a coupled effect of permeability and roughness. Therefore, examining differences in k_s values between thin and thick substrates could lead to insights on decoupling the effects of permeability from roughness. Note that some studies in the literature have used k_0 instead of k_s.

Following the work in Ref. [6] and assuming that Re_K captures the permeability effect, we can show that the mean profile is of the form,

$$U^+ = \frac{1}{\kappa}\ln\left(\frac{y+y_d}{\sqrt{K}}\right) + C_1 = \frac{1}{\kappa}\ln(y+y_d)^+ - \frac{1}{\kappa}\ln(Re_K) + C_1 \tag{4}$$

where, our data suggests that C_1 is an additive constant that depends on roughness of the substrate, which in turn depends on the thickness of the substrate and its pore-size (or porosity) as seen in figure 8a. This roughness effect can be captured via a roughness function ($\Delta {U^+}_r$) which is in addition to the permeability effect,

$$U^+ = \frac{1}{\kappa}\ln(y+y_d)^+ - \frac{1}{\kappa}\ln(Re_K) - \Delta {U^+}_r + B \tag{5}$$

Following Ref. [36], this roughness function can be modelled using the concept of sandgrain roughness, which only captures the roughness effect of the porous surface,

$$U^+ = \frac{1}{\kappa}\ln(y+y_d)^+ - \frac{1}{\kappa}\ln(Re_K) - \frac{1}{\kappa}\ln(k^+_{s_r}) + B - B'_{FR} \tag{6}$$

where k_{s_r} is the sandgrain roughness that captures only the roughness effect of the surface. This equation can be re-written as,

$$U^+ = \frac{1}{\kappa}\ln\left(\frac{y^+ + y^+_d}{k^+_{s_r} Re_K}\right) + B - B'_{FR} \tag{7}$$

This formulation now captures both the roughness effect (through k_{s_r}) and the permeability effect (through Re_K) of a given porous surface. Comparing the above equation with the definition of sand-grain roughness used to collapse the porous surface data to obtain one value of k_s as done in previous section, we find that:

$$k_s = k_{s_r} Re_K \tag{8}$$

Note that this value of k_s collapses all profiles as shown in figure 8b. Comparing thick and thin substrates of the same permeability, say 90 ppi, we find that Re_K are nearly identical at the same freestream speeds. The changes in Re_K are small compared to changes in the value of k_s. This would suggest that the permeability effect is similar between thick and thin substrates. Therefore, the difference in k_s value is entirely due to the difference in roughness k_{s_r}. The ratio of k_s between thin and thick substrates are 1.6, 2.3 and 4.8 for the three different foams (90 ppi, 45 ppi and 10 ppi) respectively. It is clear that the roughness effect increases substantially with decreasing permeability of the surface.

The current dataset (nor any other data in the literature for that matter) is not sufficient to fully capture/predict this behaviour for different thicknesses/permeabilities. However, it is hypothesised that this ratio (at matched Re_K) is a function of thickness to pore-size ratio, which would depend on the flow penetration depth. We expect this ratio to asymptote to a constant value with increasing thickness. Further experiments are required to evaluate this hypothesis.

CONCLUSION

The mean flow characteristics of a turbulent boundary layer over porous substrates has been investigated for different permeability (K) and porosity (ϵ) at a broad range of Reynolds numbers. Two different substrate thicknesses were considered for each substrate, leading to six different surface topologies. Skin friction data from a floating element drag balance and single-point hot wire velocity measurements were used to assess the aforementioned findings and the limitations of similarity laws in these flows.

In order to interpret the flow over porous surfaces in the context of smooth-/rough-walls, the log region is analysed assuming a universal value of von-Karman coefficient ($\kappa = 0.39$). This enables calculation of zero-plane displacement and equivalent sand-grain roughness that can be directly compared to rough-walls. Empirical correlations for the zero-plane displacement of the same form as in Ref. [6] are constructed for the thin and thick substrates separately, and the goodness of the fit improves when the permeability Reynolds number (Re_K) is replaced with dimensionless pore size (s^+). This is in agreement with the hypothesis in Ref. [17] who state $s^+ < 5$ should be met for roughness effects to be negligible. This suggests that the porous surfaces here are under the influence of both permeability and roughness.

The equivalent sandgrain roughness obtained from hot-wire data (k_s) collapses all velocity profiles in the logarithmic region and improves the results shown in Ref. [6]. An attempt is made to decouple permeability and roughness effects; permeability is captured by Re_K while the roughness is isolated by k_{s_r} where $k_s = k_{s_r} Re_K$. Our data suggests that the roughness effect (k_{s_r}) increases with increasing thickness for similar permeabilities. It is hypothesised that this effect will saturate over a certain thickness, however, further experiments are required to clearly identify this relationship between the thickness of porous bed and its roughness.

ACKNOWLEDGEMENTS

We gratefully acknowledge the funding from Engineering and Physical Sciences Research Council (grant ref no: EP/S013296/1) and US Airforce's European Office of Aerospace Research and Development (grant ref no: 12819250; Program Officer: Dr. Douglas Smith).

All data supporting this study will be made openly available from the University of Southampton repository upon publication.

---

* luiblaes@gmail.com
† g.bharath@soton.ac.uk

[1] M. P. Schultz and K. A. Flack, Phys. Fluids **1**, 015104 (2009)
[2] K. A. Flack and M. P. Schultz, Trans. ASME J. Fluids Engng **4**, 041203 (2010)
[3] K. A. Flack and M. P. Schultz, Phys. Fluids **10**, 101305 (2014)
[4] F. E. Teruel and Rizwan-uddin, Int. J. Heat Mass Tran. **52**, 4264–4272 (2009)
[5] K. Suga, Flow Turbulence Combust **96**, 717–756 (2016)
[6] C. Manes, D. Poggi, and L. Ridolfi, J. Fluid Mech **687**, 141 (2011)
[7] C. Efstathiou and M. Luhar, J. Fluid Mech **841**, 351 (2018)
[8] A. F. E. Zagni and K. V. H. Smith, J. Hydraul. Div **102**, HY2 (1976)
[9] F. Kong and J. Schetz, AIAA , 30 (1982)
[10] H. J. Zippe and W. H. Graf, J. Hydraul. Res. **21**, 51–65 (1983)
[11] Y. Shimizu, T. Tsujimoto, and H. Nakagawa, J. Hydrosci. Hydraul. Eng. **8**, 69–78 (1990)
[12] D. Manes, C. Pokrajac, I. Mcewan, and V. Nikora, Phys. Fluids **21**, 125109 (2009)
[13] T. Kim, G. Blois, J. L. Best, and K. T. Christensen, International Journal of Heat and Fluid Flow **73**, 16 (2018)
[14] T. Kim, G. Blois, J. L. Best, and K. T. Christensen, Journal of Hydraulic Research , 1 (2019)
[15] T. Kim, G. Blois, J. L. Best, and K. T. Christensen, Journal of Fluid Mechanics **887**, A3 (2020)
[16] J. Jimenez, M. Uhlmann, P. A., and G. Kawahara, J. Fluid Mech. **442**, 89 (2001)
[17] W. P. Breugem, B. J. Boersma, and R. E. Uittenbogaard, Journal of Fluid Mechanics **562**, 35–72 (2006)
[18] M. Chandesris, A. D'Hueppe, B. Mathieu, D. Jamet, and B. Goyeau, Phys. Fluids **25**, 125110 (2013)
[19] K. Kuwata, Y. Suga, Intl J. Heat Fluid Flow 61 (Part A) , 145–157 (2016)
[20] K. Kuwata, Y. Suga, Flow Turbulence Combust (2016)
[21] S. Hahn, J. Je, and H. Choi, J. Fluid Mech. **450**, 259–285 (2002)
[22] M. E. Rosti, L. Cortelezzi, and M. Quadrio, J. Fluid Mech **784**, 396–442 (2015)
[23] H. Fang, X. Han, G. He, and S. Dey, J. Fluid Mech **847**, 552–590 (2018)
[24] K. Kuwata, Y. Suga, J. Fluid Mech **831**, 41–71 (2017)
[25] G. Gomez-de-Segura and R. Garcia-Mayoral, Journal of Fluid Mechanics **875**, 124 (2019)
[26] E. Padhi, N. Penna, S. Dey, and R. Gaudio, Physics of Fluids **30**, 085105 (2018)
[27] X. Han, H. Fang, G. He, and D. Reible, Water Res. **129**, 39–50 (2018)
[28] G. Shen, J. Yuan, and M. Phanikumar, Journal of Fluid Mechanics **892**, A20 (2020)
[29] Y. Okazaki, A. Shimizu, Y. Kuwata, and K. Suga, IJHFF **82**, 108541 (2020)
[30] J. Jimenez, Annual Review of Fluid Mechanics **36**, 173–196. (2004)

[31] K. Suga, Y. Matsumura, Y. Ashitaka, S. Tominaga, and M. Kaneda, Intl J. Heat Fluid Flow **6**, 974 (2010)
[32] A. Clifton, C. Manes, J. D. Rüedi, M. Guala, and M. Lehning, Boundary-Layer Meteorol. **450**, 249–261 (2008)
[33] N. Hutchins, T. B. Nickels, I. Marusic, and M. S. Chong, J. Fluid Mech. **635**, 103 (2009)
[34] M. Aguiar Ferreira, E. Rodriguez-Lopez, and B. Ganapathisubramani, Exp. Fluids **59**, 155 (2018)
[35] J. P. Monty, E. Dogan, R. Hanson, A. J. Scardino, B. Ganapathisubramani, and N. Hutchins, Biofouling **32**, 451 (2016)
[36] J. Nikuradse, NACA TM , 1292 (1933)
[37] C. F. Colebrook and C. M. White, Philos Trans Royal Soc A Math Phys Eng Sci. **16**, 367–381 (1937)
[38] I. Marusic, J. P. Monty, M. Hultmark, and A. J. Smits, J. Fluid Mech **716**, R3 (2013)